



Integrated validation of assimilating satellite derived observations over France using a hydrological model

D. Fairbairn¹, A. L. Barbu^{1,2}, A. Napoly¹, C. Albergel¹, J.-F. Mahfouf¹, and J.-C. Calvet¹

¹CNRM, UMR 3589 (Météo-France, CNRS), Toulouse, France

²Now at Observatoire Midi-Pyrénées, Toulouse, France

Correspondence to: J.-C. Calvet (jean-christophe.calvet@meteo.fr)

Abstract. This study assesses the impacts of assimilating surface soil moisture (SSM) and leaf area index (LAI) observations on river discharge using the SAFRAN-ISBA-MODCOU (SIM) hydrological model. The SIM hydrological model consists of three stages: (1) An atmospheric reanalysis (SAFRAN) over France, which forces (2) a land surface model (ISBA-A-gs), which then provides drainage and runoff inputs to (3) a hydrogeological model (MODCOU). The river discharge from MODCOU is validated using observed river discharge over France from over 500 gauges. The SAFRAN forcing underestimates direct short-wave and long-wave radiation by approximately 5% averaged over France. The ISBA-A-gs model also significantly underestimates the grassland LAI compared with satellite retrievals during winter dormancy. These differences result in an underestimation (overestimation) of evapotranspiration (drainage and runoff). The excess water flowing into the rivers and aquifers contributes to an overestimation of the SIM discharge. We attempted to resolve these problems by performing the following experiments: (i) a correction of the minimum LAI model parameter for grasslands, (ii) a bias-correction of the model radiative forcing, (iii) the assimilation of LAI observations and (iv) the assimilation of SSM and LAI observations. The data assimilation for (iii) and (iv) was done with a simplified extended Kalman filter (SEKF), which uses finite differences in the observation operator Jacobians to relate the observations to the model variables. Experiments (i) and (ii) improved the average SIM Nash scores by about 12% and 20% respectively. Experiment (iii) reduced the LAI phase errors in ISBA-A-gs but only slightly improved the discharge Nash efficiency of SIM (by just 2%). In contrast, experiment (iv) resulted in spurious increases in drainage and runoff, which degraded the discharge Nash efficiency by about 35%. The poor performance of the SEKF is an artifact of the observation operator Jacobians. These Jacobians are dampened when the soil is saturated and when the vegetation is dormant, which leads to positive biases in drainage/runoff and insufficient corrections to the LAI minimum, respectively. This motivates the development of a DA method that can take into account model errors and atmospheric forcing errors. The results also highlight the important role that vegetation plays on the hydrological cycle. It is recommended that a spatially variable LAI minimum parameter be introduced into ISBA-A-gs based on the lowest LAI values derived from satellite observations.



1 Introduction

Soil moisture influences the flow of water to rivers and aquifers, which makes it an important factor in hydrological models. In the last two decades there have been considerable advances in soil moisture data assimilation (DA) using remotely sensed near-surface soil moisture (Houser et al., 1998; Crow and Wood, 2003; Reichle and Koster, 2005; Drusch and Viterbo, 2007; Draper et al., 2012; de Rosnay et al., 2013). The estimation of global-scale soil moisture states has benefitted considerably from a huge expansion of the satellite network, namely the Advanced Scatterometer (ASCAT) instrument on board the METOP satellites (Wagner et al., 2007), the Soil Moisture and Ocean Salinity (SMOS) Mission (Kerr et al., 2001) and the Soil Moisture Active Passive (SMAP) Mission (Entekhabi et al., 2010), amongst others. However, these instruments can only indirectly observe the top 1-3 cm of soil moisture and are subject to retrieval errors. There are also spatial and temporal gaps in the observation network. The aim of DA methods is to combine these observations with a short forecast from the past (the background state) to provide an improved estimate of the soil moisture state (the analysis). DA methods are necessary to account for the errors in the observations and the land surface model (LSM), and to spread the information from the surface to the deeper layers. Typically the root-zone soil moisture (WG2) (1-3 m deep) is of more interest than the SSM as it has a much larger water capacity and therefore has a greater influence on vegetation and water fluxes.

The vegetation influences the soil moisture state through evapotranspiration and the vegetation coverage can be estimated by the leaf area index (LAI). This is a dimensionless quantity that represents the one-sided green leaf area per unit ground surface area (Gibelin et al., 2006). Comparisons with observations suggest that the LSM at Météo-France can skillfully capture seasonal changes in LAI, although significant phase and amplitude errors are common for some vegetation types (Jarlan et al., 2008; Brut et al., 2009; Barbu et al., 2014). The LAI can be derived from satellite measurements in the visible range. However, over France it is available from polar-orbiting satellites at a relatively low temporal frequency (on average every 10 days) compared with soil moisture satellite observations (about every 3 days) due to cloud cover.

A Simplified Extended Kalman Filter (SEKF) is part of the surface externalised (SURFEX) modelling platform of Météo-France (Mahfouf et al., 2009; Masson et al., 2013). The SEKF is currently not coupled with an NWP model at Météo-France, but is used for other applications, such as the European Copernicus programme (<http://land.copernicus.eu/global/>, last accessed March 2016). The European Centre for Medium range Weather Forecasts (ECMWF) have coupled an SEKF with their NWP model for the assimilation of screen-level temperature and humidity (de Rosnay et al., 2013), and for the assimilation of ASCAT SSM observations since April 2015 (Patricia de Rosnay, personal communication). At Météo-France, a multi-variate SEKF has been used for the joint assimilation of SSM and LAI (Barbu et al., 2014). The SEKF assumes that the errors in the background state are fixed and uses finite differences for computing Jacobians necessary to extract information from the observations to the prognostic variables (WG2 and LAI) over the French domain. Several studies have shown that generally the SEKF improves on the ISBA model estimates of WG2 and LAI (see e.g. Muñoz Sabater et al. (2008); Albergel et al. (2010a); Barbu et al. (2011, 2014)). In particular, Barbu et al. (2014) used the same observation datasets and a similar setup as were used in this study. They found that the WG2 and LAI states over France were enhanced by the assimilation. However, the SEKF finite difference approach is based on linear assumptions, which can be inaccurate, especially near the the soil moisture thresholds



(Draper et al., 2011; Duerinckx et al., 2015; Fairbairn et al., 2015). Also, the SEKF is not designed to take into account model errors and atmospheric forcing errors. These deficiencies can lead to imbalances in the soil moisture fluxes (drainage, runoff and evapotranspiration) (Draper et al., 2011).

In this study we explore the influence of both the assimilation of SSM and LAI satellite derived observations on the river discharges simulated by the SAFRAN-ISBA-MODCOU (SIM) hydrological model over France. The SSM observations are retrieved from ASCAT data and the LAI observations are derived from the European Copernicus global land (GEOV1) satellite data. The SIM model consists of three stages: (1) An atmospheric analysis (SAFRAN) over France, which forces (2) a land surface model (ISBA), which then provides drainage and runoff inputs to (3) a hydrogeological model (MODCOU). The MODCOU model then estimates river discharge and aquifer levels (Ledoux et al., 1989). Since 2003, SIM has been used operationally by Météo-France to monitor water resources in near real time (Habets et al., 2008).

This work is partly motivated by the study of Draper et al. (2011), who investigated the influence of assimilating SSM on SIM over France. They used SIM with atmospheric forcing based on a near real time reanalysis from SARFRAN for the SEKF. They then used SIM with improved atmospheric forcing from a delayed cut-off time reanalysis from SAFRAN to validate the performance of the SEKF. It was found that the assimilation of unbiased SSM observations led to spurious increases in drainage and runoff fluxes, which then increased the SIM river discharge. They therefore recommended correcting the errors in the atmospheric forcing directly, rather than trying to rectify the resulting soil moisture errors with DA. Studies by Szczypta et al. (2011) and Bertrand Decharme (personal communication) have found underestimations of about 5% by SAFRAN in the direct short-wave and long-wave radiative fluxes respectively, averaged over France. In addition to these problems with radiative forcing, we found in this study that the LSM significantly underestimates LAI for grasslands in winter (compared with satellite retrievals). The specification of the LAI minimum in the model is important because it prevents vegetation mortality and allows the regrowth of vegetation in the spring period (Gibelin et al., 2006). We also noticed phase errors in the dynamic model evolution of LAI. We use SIM as a tool to validate potential solutions to these deficiencies, based on four experiments:

- i. Correcting the model under-estimated LAI minimum parameter;
- ii. Bias-correcting the SAFRAN radiative forcing;
- iii. Assimilating only LAI observations with an SEKF;
- iv. Assimilating SSM and LAI observations with an SEKF.

Since Draper et al. (2009) already investigated the impact of assimilating SSM on SIM, it was not necessary to perform an experiment with the assimilation of SSM only. We validate the performance of these experiments using observations from more than 500 river gauges over France during the period July 2007 to August 2014.

It should be kept in mind that the purpose of DA is to improve the state of the system at the current time. This explains why DA works particularly well for chaotic systems such as atmospheric models, where errors in the initial conditions dominate forecast errors. However, LSMs are not chaotic and most of the errors are generated from accumulations of errors in the model



and the atmospheric forcing. But studies with LSMs have demonstrated that DA can effectively reduce errors in the model state that are caused by deficiencies in the model and the atmospheric forcing. For example, Albergel et al. (2010a) demonstrated that the assimilation of SSM can correct a dry bias in the root-zone soil moisture that was introduced by an underestimation in the precipitation forcing. Furthermore, Barbu et al. (2014) demonstrated that the assimilation of LAI reduces the phase errors in the modelled LAI evolution. In this study the SSM observations are rescaled such that the mean and standard deviation match the model climatology. Therefore we would not expect the assimilation of SSM observations to significantly impact the errors caused by the systematic model and forcing deficiencies in this study. Nevertheless, the assimilation of the SSM observations is designed to correct short term errors in the model evolution and should therefore impact SIM. The LAI observations are not rescaled, so it is reasonable to examine whether the assimilation of LAI can impact the systematic model and forcing deficiencies, as well as the short term errors. We repeat experiments (iii) and (iv) after correcting the LAI minimum and the radiative forcing in order to explore other potential impacts of the DA on SIM.

The paper is structured as follows. The methods and materials are given in Sect. 2, which includes a description of the observations, the SIM model and the DA methods. The results are presented in Sect. 3, including the impact of the model simulations and DA on the model state variables and the river discharge. A discussion in Sect. 4 considers potential solutions to the problems encountered in this study. Finally, the conclusion is given in Sect. 5.

2 Methods and materials

2.1 SIM hydrological model

A complete description and validation of SIM can be found in Habets et al. (2008). In our study, the LSM was forced by the atmospheric variables provided by the “Système d’Analyse Fournissant des Renseignements à la Neige” (SAFRAN). The SAFRAN forcing is derived from a meso-scale analysis system and is assumed to be homogeneous over 615 specified climate zones. The forcing is interpolated from these zones to the Lambert projected grid with a horizontal resolution of 8 km (Durand et al., 1993). The delayed cut-off version of SAFRAN was employed, which uses observations from more than 1200 automatic weather stations and an additional 3000 climatological observing stations (which report one-monthly) over France (Quitana-Ségui et al., 2008; Vidal et al., 2010). The atmospheric variables include precipitation, wind, incoming short-wave and long-wave radiation, relative humidity and air temperature with an hourly temporal sampling.

Version 8.0 of SURFEX was used in the experiments, which contains the “Interactions between Soil, Biosphere and Atmosphere” (ISBA) LSM (Noilhan and Mahfouf, 1996). The model uses the same horizontal grid resolution as SAFRAN of 8 km. The ISBA-A-gs version was used, which allows for the influence of leaf-scale physiological processes, including photosynthesis (Calvet et al., 1998). Each grid cell is split into twelve land cover types (so called “patches”). Soil and vegetation parameters are derived from the ECOCLIMAP database (Faroux et al., 2013). The nitrogen dilution version (referred to as “NIT” hereafter) of ISBA-A-gs was used in the experiments, which dynamically simulates the LAI evolution (Gibelin et al., 2006). The NIT version allows for the effects of atmospheric conditions on the LAI, including the carbon dioxide concentrations.



The three-layer version of ISBA was adopted for this study (Boone et al., 1999). This includes the WG1 layer with depth 1cm. The WG2 layer includes WG1 and is 1-3 m deep, with the depth depending on the patch type. A recharge zone exists below WG2. The model water transfers are governed by the force-restore method of Deardorff (1977). The surface and root zone layers are forced by the atmospheric variables and restored towards an equilibrium value. The drainage and runoff outputs from ISBA-A-gs drive the MODCOU hydrogeological model. The gravitational drainage is proportional to the water amount exceeding the field capacity (the effective limit where gravitational drainage ceases) (Mahfouf and Noilhan, 1996). It is driven by the hydraulic conductivity of the soil, which depends on the clay content. A small residual drainage below the field capacity was introduced by Habets et al. (2008) to account for unresolved aquifers. Runoff occurs when the soil moisture exceeds the saturation value.

The MODCOU hydrogeological model (Ledoux et al., 1989) uses drainage and runoff from ISBA-A-gs to compute the daily evolution of aquifer storages and three-hour river flow forecasts. More than 900 river gauges are simulated with areas ranging from 240 km² to 112,000 km². Aquifers in the Rhone and Seine Basins are also simulated. The influence of human activity, such as dams and irrigation, is not accounted for by MODCOU.

2.2 Observations

The SSM observations are retrieved from ASCAT radar observations, which observe at 5.255 GHz (C-band) and a resolution of approximately 25 km. The radar is on board EUMETSAT's Meteorological Operational (MetOP) satellite. The original ASCAT values are converted into SSM values using a change detection technique, which was developed at the Vienna University of Technology (Tu-Wien) and is detailed in Wagner et al. (1999); Bartalis et al. (2007). The Copernicus Global Land Service then converts these SSM observations into the soil water index (SWI) equivalent, which ranges between 0 (dry) and 1 (saturated). The SWI-001 version 2.0 product is used in this study. It is generated from an exponential filter with a characteristic time length of one day, which is representative of the first few centimetres of soil. We then interpolate the SWI-001 data to the 8 km resolution model grid. As in Draper et al. (2011) an additional screening step is performed to remove observations with an altitude greater than 1500m, frozen regions and areas with an urban fraction greater than 15%.

We apply a linear rescaling to the SWI-001 data, which scales them such that the mean and standard deviations match the WG1 layer climatology (Calvet and Noilhan, 2000; Scipal et al., 2008). This is a linear approximation of the cumulative distribution matching technique, which uses higher order moments (Reichle et al., 2004; Drusch et al., 2005). As in Barbu et al. (2014), we apply a seasonal rescaling using a 3-month moving average over the experiment period (2007-2014). The rescaling is designed to remove biases between the model and the observations and in the process the SWI-001 data are converted into the same units as the model, expressed in volumetric soil moisture (m³/m³). These rescaled SSM observations are assimilated into the WG1 model layer. The observations are assumed to occur at the same time as the analysis at 09UTC. This is a reasonable assumption since the satellite overpass is at 09:30 UTC. They have an average temporal frequency of about 3 days.

The GEOV1 LAI product is part of the European Copernicus GEOLAND 2 project. The LAI observations are retrieved from the SPOT-VGT (August 2007 to June 2014) and PROBA-V (June 2014-July 2014) satellite data. The retrieval methodology is discussed by Baret et al. (2013). Following Barbu et al. (2014), the 1 km resolution observations are interpolated to the 8



km model gridpoints, provided that observations are present for at least 32 of the observation gridpoints (just over half the maximum amount). The observations are assumed to occur at 09UTC with a temporal frequency of 10 days. This assumption is reasonable given that LAI evolves slowly.

The daily river discharge observations, which are used to validate the SIM performance, come from river gauges and are available from the French hydrographical database (<http://www.hydro.eaufrance.fr/>, last accessed March 2016). The validation of SIM was based on 546 river gauges that had data during the period of evaluation (2007-2014). The average daily river discharge from the observations (measured in $\text{m}^3/\text{m}^3\text{s}^{-1}$) is compared with the average daily river discharge from MODCOU.

2.3 Data assimilation

The SEKF simplifies the extended Kalman filter (EKF, (Jazwinski, 1970)) by using a fixed estimate of the background-error variances at the start of the window and by assuming the covariances are equal to zero (Mahfouf et al., 2009). We use the same SEKF formulation as Barbu et al. (2014) for the assimilation of SSM and LAI observations over France. The prognostic variables are LAI and WG2. The background state (\mathbf{x}^b) at time t_i is a model propagation of the previous analysis ($\mathbf{x}^a(t_{i-1})$) to the end of the 24 hour assimilation window:

$$\mathbf{x}^b(t_i) = M_{i-1}(\mathbf{x}^a(t_{i-1})), \quad (1)$$

where M is the (nonlinear) ISBA-A-gs model. The observation is assimilated at the analysis time, at 09UTC, at the end of the 24-hour assimilation window. The analysis is calculated from the generic Kalman filter equation:

$$\mathbf{x}^a(t_i) = \mathbf{x}^b(t_i) + \mathbf{K}_i(\mathbf{y}_i^o - \mathbf{y}_i), \quad (2)$$

where \mathbf{y}^o is the assimilated observation and $\mathbf{y}_i = H(\mathbf{x}^b(t_i))$ is the model predicted value of the observation at the analysis time. The Kalman gain is defined as:

$$\mathbf{K}_i = \mathbf{B}_i \mathbf{H}_i^T (\mathbf{H}_i \mathbf{B}_i \mathbf{H}_i^T + \mathbf{R}_i)^{-1}, \quad (3)$$

where \mathbf{H} is the Jacobian matrix of the linearized observation operator, \mathbf{B} is the background-error covariance matrix and \mathbf{R} is the observation-error covariance matrix. The observation operator Jacobians are calculated using finite differences for observation k and model variable l :

$$\mathbf{H}_i^{kl} = \frac{H_i^k(M_{i-1}(\mathbf{x}(t_{i-1}) + \Delta x_{i-1}^l) - H_i^k(M_{i-1}(\mathbf{x}(t_{i-1}))))}{\Delta x_{i-1}^l}, \quad (4)$$

where Δx^l is a model perturbation applied to model variable l . Following Draper et al. (2009), the WG2 perturbation was set to $1.0 \times 10^{-4} \text{ m}^3/\text{m}^3$ and in accordance with Rüdiger et al. (2010), the LAI perturbation was set to $1.0 \times 10^{-3} \text{ m}^2/\text{m}^2$. Equation (4) requires an additional model simulation for each prognostic variable. The linear assumptions in deriving the Jacobians are generally acceptable for these perturbation sizes. However, occasionally the linear assumptions can break down, especially during dry periods in summer (Draper et al., 2009; Fairbairn et al., 2015). For this reason we have set an upper bound on the



Jacobians of 1.0. It is worth mentioning that in situations where the model and atmospheric forcing errors are not properly taken into account the SEKF analysis will be suboptimal even if the Jacobian calculation is accurate enough. The Jacobian matrix derived from Eq. (4) is defined as follows:

$$\mathbf{H} = \begin{pmatrix} \frac{\partial \text{WG1}}{\partial \text{WG2}} & \frac{\partial \text{WG1}}{\partial \text{LAI}} \\ \frac{\partial \text{LAI}}{\partial \text{WG2}} & \frac{\partial \text{LAI}}{\partial \text{LAI}} \end{pmatrix}. \quad (5)$$

- 5 When assimilating just LAI, only the $\frac{\partial \text{LAI}}{\partial \text{WG2}}$ and $\frac{\partial \text{LAI}}{\partial \text{LAI}}$ terms are included. The $\frac{\partial \text{WG1}}{\partial \text{LAI}}$ is generally small, since the LAI does not substantially influence the surface layer (Barbu et al., 2014). The $\frac{\partial \text{WG1}}{\partial \text{WG2}}$ Jacobian couples WG1 with WG2 (Draper et al., 2009). The $\frac{\partial \text{LAI}}{\partial \text{WG2}}$ couples LAI with WG2 (Barbu et al., 2014). The $\frac{\partial \text{LAI}}{\partial \text{LAI}}$ Jacobian was studied by Rüdiger et al. (2010) and has a strong seasonal dependence. As we will demonstrate in Sect. 3.3, the examination of these Jacobians is essential in order to understand the performance of the SEKF.
- 10 SURFEX is implemented using the mosaic approach of Koster and Suarez (1992), where each model grid-box is split into 12 vegetation patches. The SEKF analysis is calculated independently for each patch, with the same observation used for all the patches in the grid-box. The analysis for the gridpoint is simply a linear aggregation of the analyses over the 12 patches, which are weighted according to their patch fractions (see Barbu et al. (2014) for further details).

The WG2 background and WG1 observation error standard deviations are prescribed values of $0.2(w_{fc}-w_{wilt})$ and $0.4(w_{fc}-w_{wilt})$ respectively, where w_{fc} is the field capacity and w_{wilt} is the wilting point. These are similar to the values used by Mahfouf et al. (2009) and the scaling by $(w_{fc}-w_{wilt})$ assumes that there is linear relationship between the soil moisture errors and the dynamic range. As in Barbu et al. (2011) the LAI background and observation error standard deviations are proportional to the LAI values themselves and a value of $0.2 \times \text{LAI}$ is used for LAI values greater than $2 \text{ m}^2/\text{m}^2$. For LAI values below $2 \text{ m}^2/\text{m}^2$ the LAI errors are fixed at $0.4 \text{ m}^2/\text{m}^2$. Both the background-error and observation-error covariance matrices are diagonal (zero covariances between layers), but implicit background-error covariances are derived from the \mathbf{H} matrix at the analysis time. The SEKF is a pointwise method i.e. it cannot take into account horizontal covariances between gridpoints.

2.4 Experimental setup

The main experiments in this study are summarised in Table 1. This list includes the baseline experiment (NIT), which demonstrates the impact of the biased radiative forcing and the under-estimated LAI minimum on the SIM river discharge. Thereafter, various potential solutions to these deficiencies are investigated, as set out in the introduction: (i) NIT_m , which is equivalent to NIT but with an elevated LAI minimum of $1.2 \text{ m}^2/\text{m}^2$ for grasslands (as opposed to $0.3 \text{ m}^2/\text{m}^2$ with NIT), (ii) NIT_{bc} , which uses both the elevated LAI minimum of $1.2 \text{ m}^2/\text{m}^2$ and the bias-corrected radiative forcing (+5% for direct long-wave and short-wave over France), (iii) LDAS1, which uses the SEKF to assimilate LAI only with the NIT model and (iv) LDAS2, which assimilates both LAI and SSM observations with the NIT model.

30 Three additional experiments in Table 1 explored whether SSM observation outliers, the under-estimated LAI minimum or the radiative forcing bias might impact the performance of the DA. The LDAS2_{QC} is equivalent to LDAS2 but with a strict quality control of the SSM observations to remove any abnormal outliers due to instrument noise. The outliers were removed by



rejecting observations outside the 90% confidence interval of the model (as in Eq. (1) and (2) of Albergel et al. (2010b)) after the observations had been rescaled. The LDAS1_{bc} and LDAS2_{bc} experiments are equivalent to LDAS1 and LDAS2 respectively, except they use the NIT_{bc} model. The SSM observations for LDAS2_{bc} were rescaled such that the standard deviation and mean matched those of NIT_{bc}.

- 5 The LAI and WG1 state estimates for the experiments are validated using the satellite observations. Their fit to the observations is determined by the root mean square difference (RMSD), the correlation coefficient (CC) and the bias. The SIM river discharge is then validated using the river gauge observations in terms of the Nash efficiency score (Nash and Sutcliffe, 1970). The Nash efficiency can range from $-\infty$ to 1, with 1 corresponding to a perfect match of the model to the observed data and scores less than zero implying that the model mean is a worse predictor than the observations. Following Habets et al. (2008)
- 10 we consider an efficiency of 0.6 to be a good score and 0.5 to be a reasonable score. The validation period extends from August 2007 to July 2014, with the hydrological year running from August to July.

The SIM domain consists of 9892 gridpoints, of which 8602 are based in France. The remaining 1290 points are based in mountainous regions bordering the French mainland, including most of Switzerland (see Habets et al. (2008) for details). The LSM does not model horizontal exchanges, but MODCOU takes into account horizontal river flow. Therefore it is important

15 to include these external points because they impact the river discharge over France, particularly in the Rhone basin in the southeast. The SEKF only assimilates observations over the 8602 points in the LDAS France domain. Figure 1 shows a flowchart of SIM and how LDAS France is connected with ISBA-A-gs in SIM. Figure 2 shows the river network used by MODCOU and the stations used to validate the discharge.

3 Results

20 3.1 Impact of model and forcing bias-corrections on SIM

To begin with we examine the influence of the different model simulations on the LAI evolution for the four dominant vegetation patches. We will then link the hydrological performance to each simulation. Over France, the four dominant vegetation patches are grasslands (32%), C3 croplands (24%), deciduous forests (20%) and coniferous forests (12%). Fig. 3 shows the monthly averaged LAI model simulations and observations for the gridpoints that contain at least 50% of the dominant vege-

25 tation types. The 50% threshold was used because very few points contain more than 70% of any vegetation type, while over 1000 gridpoints contain at least 50% of any vegetation type. Table 2 shows the average LAI scores over France (RMSD, CC and bias) for each of the model simulations.

Firstly we examine the LAI performance for the NIT simulation, which dynamically estimates the LAI evolution. Fig. 3 shows that the NIT simulation is close to the observations for the deciduous forests (Fig. 3(a)). However, the growth and senescence phases are delayed for the simulated C3 crops and grasslands (Fig. 3(c) and (d)) compared with the observations. Furthermore, the grassland LAI is significantly underestimated by NIT in winter. It is clear in Fig. 3 that imposing this higher minimum LAI value (NIT_m) significantly increases the LAI for grasslands_m in winter and improves the fit to observations. This is reflected by better scores for NIT_m compared with NIT. Fig. 4 shows the average annual LAI minimum for NIT, NIT_m

30



and the observations over France. The effect of imposing the higher LAI minimum on NIT is apparent over most regions, especially in the predominantly grassland regions of central southern France. This augmented LAI minimum better matches the observations than the default minimum. Finally, the benefit of the bias-correction (NIT_{bc}) on LAI is also demonstrated in Fig. 3. The bias-correction has little impact on the LAI of the deciduous and coniferous forest patch types. However, it does
5 reduce the phase errors for both the C3 crops and grassland patches. This results in significantly better LAI scores, reducing (increasing) the RMSD (CC) by about 10% compared with NIT.

The WG1 scores for the various simulations are given in Table 3. Recall that the SSM observations are linearly rescaled such that their mean and standard deviation match the NIT model simulation of WG1, which removes any bias already present. Changing the model simulation has little impact on the scores, which suggests that the LAI evolution and the radiative forcing
10 have a relatively small influence on the moisture content of the surface layer.

Next, the Nash efficiency scores for the different model simulations are displayed in Fig. 5 (a), showing the percentage of gauging stations at efficiency scores between 0 and 1.0. With the NIT simulation, about 30% of the stations have a score above 0.6 (a good score). About 40% of the stations have a score above 0.5 (a reasonable score). About 20% of the stations have a negative Nash score. The Nash efficiency for NIT for each station over France is shown in Fig. 2. The river discharge is well
15 simulated over most areas, but the southeast and northern regions have generally negative scores (shown in black). In southeast France this is related to a large number of dams in the alps, which are not simulated by MODCOU. In northern France, this is linked to a large aquifer that is also not taken into account by MODCOU (see Habets et al. (2008) for details). The negative scores in these regions are not linked to a bias (not shown). The NIT_m simulation in Fig. 5 (a) leads to an improved Nash scored compared to NIT, with about 35% of stations reaching a score of 0.6 and 45% of stations with a score of 0.5 or higher.
20 Then introducing bias correction (NIT_{bc}) further enhances the Nash scores. Table 4 shows the average Nash scores for each simulation, but only includes stations where at least one of the experiments has a positive score. Therefore most of the stations in northern and southeast France are excluded from this calculation. The average Nash scores for NIT_m and NIT_{bc} are 12% and 20% higher than NIT, respectively. The discharge ratio between the modelled (Q_s) and observed (Q_o) discharge is also shown for each simulation. A value that is greater (smaller) than 1.0 indicates a positive (negative) bias in the model. NIT has
25 a discharge ratio of 1.19, which is reduced to 1.15 by applying the LAI minimum and further reduced to 1.02 by applying the bias-correction. Therefore it appears that the bias in the discharge ratio has an important impact on the Nash score, with larger biases corresponding to smaller Nash scores. This is clarified when comparing the annual Nash scores (Fig. 6(a)) with the annual discharge ratios in (Fig. 6(b)). It is clear that the size of the bias in the discharge ratio is negatively correlated with the Nash score. This explains why NIT_{bc} performs so well, especially between 2009 and 2013. Fig. 6(c) and (d) show the average
30 annual temperature and rainfall respectively. There does not appear to be a strong correlation between either the temperature or rainfall and the Nash score.

Finally, we investigate the influence of the model simulations on the drainage and runoff fluxes in order to explain the differences in the SIM discharge. Fig. 7(a)-(e) show the average monthly LAI, WG2, evapotranspiration, drainage and runoff respectively, averaged over France. We start by comparing NIT and NIT_m , since these simulations only differ in the way that
35 LAI is modelled. NIT_m has a greater average LAI in winter than NIT because the NIT LAI minimum is under-estimated.



The effect of a higher LAI is to enhance evapotranspiration, which reduces the soil moisture and therefore diminishes the drainage and runoff. Figure 3(f) shows the difference between the sum of drainage and runoff for the different simulations compared with NIT. It is clear that NIT_m has less drainage and runoff than NIT from October to June. The NIT_{bc} simulation increases the radiative forcing by 5%, which results in increased evapotranspiration and lower WG2 during the year. This significantly reduces the drainage and runoff from October to June. These findings agree with the results from Table 4 showing that increasing the minimum LAI (NIT to NIT_m) and radiative forcing (NIT_m to NIT_{bc}) both reduce the MODCOU discharge bias, which consequently improve the Nash scores.

3.2 Impact of DA on SIM

The performance of the DA runs on the LAI and WG1 scores are shown in Tables 2 and 3 respectively. LDAS1 significantly improves the fit to the observations compared to NIT. We investigate the influence of DA on the drainage and runoff fluxes in Fig. 8, which shows the same variables as Fig. 7. Fig. 8(b) demonstrates that the assimilation of LAI reduces the LAI phase errors in NIT. Therefore LDAS1 has much better LAI scores than any of the other experiments. However, the LAI assimilation does not address the problem of the underestimated LAI in winter, unlike LAI_m in Fig. 7(b). The LAI assimilation has a relatively small influence on the water fluxes. The small positive correction of LAI in spring helps to slightly increase evapotranspiration and therefore reduce drainage and runoff during this period. For this reason LDAS1 slightly reduces the discharge bias compared to NIT (Fig. 5(b) and Table 4) and therefore marginally improves the Nash discharge efficiency scores. LDAS1 does not significantly influence the WG1 scores because LAI has a relatively small impact on the surface layer.

The LAI results for LDAS2 are fractionally worse than for LDAS1, but still significantly better than the NIT simulation. However, LDAS2 does slightly improve the WG1 scores relative to NIT. The Nash discharge scores are degraded by about 35% for LDAS2 compared to NIT (Fig. 5(b) and Table 4) and the positive bias in the discharge ratio is increased by about 8% (Table 4). The reason for this is that LDAS2 causes an increase in WG2 (Fig. 5(b)), which translates to augmented drainage and runoff for LDAS2 relative to the NIT simulation (Fig. 8(f)). The extra water in the rivers exacerbates the Nash discharge bias already present, resulting in poor Nash efficiency scores.

3.3 Examining the SEKF Jacobians

The SEKF Jacobians are governed by the physics of the model. Their examination is important in order to understand the SEKF performance. The behaviour of the $\frac{\partial \text{LAI}}{\partial \text{LAI}}$ Jacobian values for ISBA-A-gs were investigated by Rüdiger et al. (2010). Their behaviour can be split into three distinct types, which depend on the atmospheric conditions. The type “O” Jacobian is strictly equal to zero and occurs mainly in the winter when the vegetation is dormant. In this case the LAI will instantaneously return to its default model minimum. The type “A” Jacobian represents a fraction between zero and one and is correlated with the LAI value itself. It occurs during periods of vegetation growth i.e. predominantly in spring. The type “B” Jacobian is equal to 1.0 and takes place during periods of low vegetation growth or high mortality, which occurs mainly in autumn. The grassland Jacobians are plotted for LDAS1 in Fig. 9 for a particular point in southwest France (43.35° N, 1.30° E). Also plotted in the same graph are the LAI values themselves, with the minimum indicated by the red line. Indeed, the type O Jacobians tend to



occur in winter, during which time the LAI instantaneously returns to its minimum value of $0.3 \text{ m}^2/\text{m}^2$. The type A and B Jacobians tend to occur in spring and autumn respectively. These findings are in agreement with Fig. 4 of Rüdiger et al. (2010). The LAI performance for LDAS1 can now be explained by these Jacobian values. Figure 8(b) shows that during the winter the lowest LAI values are barely corrected by LDAS1 because, as shown in Fig. 9, the LAI is frequently forced back to its minimum value (type O Jacobians). During the spring there is a small correction (type A Jacobians) and during the autumn there is a much larger correction (type B Jacobians). Hence the LDAS1 is able to correct the LAI phase errors to some extent, but LDAS1 is unable to correct the LAI minimum in winter. Since most of the drainage and runoff is present in winter and spring, the assimilation of LAI has little influence on SIM. Therefore it is much more effective to correct the LAI minimum parameter for grasslands directly than to correct the minimum using DA.

10 The $\frac{\partial \text{LAI}}{\partial \text{WG2}}$ Jacobian has generally positive values, since an increase in water content in the soil generally enhances photosynthesis and plant growth (not shown). However, this term is close to zero from about November to March while the vegetation is dormant. Therefore it does not significantly influence the LAI minimum in winter.

The WG2 analysis increments for LDAS2 are largely driven by the $\frac{\partial \text{WG1}}{\partial \text{WG2}}$ Jacobian. A scatter plot of these Jacobian values against the WG1 variable is shown in Fig. 10 for the same point as Fig. 9 in Southwest France. The density of the points is derived from the kernel density estimation of Scott (1992). There are two dense regions when WG1 is equal to 0.15 and 0.30 m^3/m^3 , which occur because WG1 is a thin layer, and therefore most of the time it is either dry or close to saturation. The WG1 and $\frac{\partial \text{WG1}}{\partial \text{WG2}}$ values are negatively correlated, with larger values of WG1 corresponding to smaller values of $\frac{\partial \text{WG1}}{\partial \text{WG2}}$. This implies that when rain is detected in the model but not in the SSM observations, the analysis increment will be smaller than when the rain is missed by the model but detected by the observations. Indeed, the average WG2 analysis increment for a positive innovation is $1.0 \times 10^{-3} \text{ m}^3/\text{m}^3$, while the average increment for a negative innovation is $-0.6 \times 10^{-3} \text{ m}^3/\text{m}^3$. This imbalance in the analysis increments leads to a net uptake of water in WG2, which induces the positive bias in the SIM river discharge. This problem was already highlighted by Draper et al. (2011). The Jacobians exhibited similar patterns of behaviour for other vegetation types than grasslands and across other points in France, albeit with different magnitudes (not shown).

3.4 Additional experiments

25 Additional experiments were performed to examine whether the poor performance of the SEKF was related to other factors than the Jacobians, namely the quality control of the observations, the underestimated LAI minimum or the bias in the atmospheric forcing. It is evident in Tables 2 to 4 that applying the additional quality control of the SSM observations (LDAS2_{QC}) does not significantly modify the LAI, WG1 or Nash discharge scores compared to LDAS2, despite removing about 10% of the SSM observations. Figure 11(a) shows only small differences in the Nash efficiency percentages between LDAS2 and LDAS2_{QC}.
 30 As expected, the LDAS1_{bc} and LDAS2_{bc} experiments improved on the LAI scores of LDAS1 and LDAS2 (Tables 2), but did not improve on the WG1 scores in Table 3. These changes are a similar order of magnitude to the improvement of NIT_{bc} over NIT. In terms of discharge Nash efficiency scores, LDAS1_{bc} performed similarly to NIT_{bc} and LDAS2 performed significantly worse than NIT_{bc} (Table 4). The Nash efficiency percentages are shown in Fig. 11(b). The comparison between LDAS1_{bc} and



LDAS1_{bc} with NIT_{bc} in Fig. 11(b) is analogous to the comparison between LDAS1 and LDAS2 with NIT in Fig. 5(b). These results confirm that the inability of the SEKF to improve the soil moisture fluxes is an artifact of the SEKF Jacobians.

4 Discussion

The results from our study demonstrate that it is possible for the SEKF to improve the WG1 and LAI states, while degrading drainage and runoff fluxes. This problem is related to model and atmospheric forcing errors, which are not represented by the SEKF Jacobians.

Firstly, we examine the inability of LDAS1 to correct the lowest LAI values during winter dormancy. The LAI Jacobian ($\frac{\partial \text{LAI}}{\partial \text{LAI}}$) was frequently equal to zero during winter and therefore the LAI returned instantaneously to its incorrect minimum value after the analysis update. These Jacobian values are physically sensible, since the vegetation is dependent on the atmospheric conditions and is often dormant during the winter period. The problem is related to the lack of a model error term in the SEKF. The lowest LAI values could be corrected further with a full EKF and a model error term, but it would be complicated to parameterize the model-error covariance matrix because the LAI minimum is linked to several factors concerning the atmospheric conditions and the vegetation type. Moreover, LAI is only assimilated every 10 days so the model LAI would drift back to its underestimated minimum value between cycles. An effective and far simpler alternative was demonstrated in the experiments, which is to impose a higher LAI minimum parameter in the model.

Secondly, we examine the poor performance of LDAS2. It is important to point out that it is physically sensible for WG1 to decouple from WG2 during precipitation events. The precipitation forcing leads to a saturation of the surface layer and subsequently WG1 becomes less dependent on WG2. However, in periods when there is no rain the $\frac{\partial \text{WG1}}{\partial \text{WG2}}$ Jacobian should actually increase with soil moisture because of faster water transfers (the hydraulic conductivity is proportional to the soil moisture above the field capacity). Therefore the negative correlation between the $\frac{\partial \text{WG1}}{\partial \text{WG2}}$ Jacobian and WG1 in Fig. 10 is not entirely realistic. As recognised by Draper et al. (2011), the principal problem is that the SEKF fails to capture the uncertainty in the model and the precipitation forcing, which should increase during precipitation events and therefore compensate for the smaller Jacobians. The SAFRAN precipitation forcing performs well for a mesoscale analysis and has a higher spatial resolution than global satellite products such as ERA-interim (Quitana-Ségui et al., 2008; Vidal et al., 2010). However, by design the precipitation is assumed to be homogeneous over 615 specified climate zones. Errors are therefore introduced from the spatial heterogeneity of the precipitation, particularly in mountainous regions (Quitana-Ségui et al., 2008). Even when the precipitation is accurately represented by SAFRAN, the transfer of this information to WG2 relies on the accuracy of the land surface model. One feature that is lacking from the three-layer model is vertical variability in WG2. Parrens et al. (2014) tested the SEKF with a multi-layer diffusion model (ISBA-DIF, (Decharme et al., 2011)) over a bare soil site in southwest France, which they implemented with 11 layers. They found that WG1 increments would gradually influence the deeper layers and smaller rainfall events sometimes went undetected at the bottom layer. They also found that assimilating SSM observations into a slightly deeper layer (1-5 cm depth) than the 1 cm surface layer in this study improved the SEKF performance because



this deeper layer better represents the SSM observations (measuring 0-6 cm depth). Work is underway to test the SEKF with a more recent version of SIM (see below), which includes the ISBA-DIF multi-layer model.

It is arguably not sensible to assimilate SSM observations with the SEKF if it has rained during the past 24 hours, since the WG1 layer will be more influenced by the precipitation forcing than by WG2 (from capillarity rises). The degradation of the soil moisture fluxes by our LDAS2 experiment could be relieved to some extent by using a full EKF with a model error term, but it would be complicated to parameterize this model error term to capture model and precipitation uncertainty. An alternative method is the ensemble Kalman filter (EnKF, Evensen (1994)), which captures the uncertainty in the background with the ensemble spread. The EnKF can be designed to stochastically capture model and precipitation errors (Maggioni et al., 2012; Carrera et al., 2015). The development of an EnKF with this capability is already underway at Météo-France, with provisional tests having been carried out over 12 points (Fairbairn et al., 2015).

A problem with the SEKF that has been overlooked in this study is the accuracy of the linearity assumptions in deriving the Jacobians. It is well known that with the three-layer ISBA-A-gs model that we employed the SEKF linear assumptions are generally accurate, but during dry conditions in summer the $\frac{\partial \text{WG1}}{\partial \text{WG2}}$ Jacobian can be excessive. This is linked to a rapid increase in transpiration when water is added to WG2 following dry conditions (Draper et al., 2009; Fairbairn et al., 2015). It is worth noting that the EnKF is also affected by nonlinearity issues during these conditions (Fairbairn et al., 2015). The origin of this nonlinearity is partly related to an unrealistic feature of the surface energy balance. One single surface temperature is used to represent the vegetation and the surface layer, which causes the transpiration to increase too quickly after water is added to WG2 (Draper et al., 2009; Mahfouf, 2014). This problem could be relieved to some extent by introducing the new version of ISBA with a multiple energy balance (ISBA-MEB). Nonlinearity problems more generally could be resolved by using a DA method that captures non-Gaussian background errors, such as a particle filter. Moradkhani et al. (2012) demonstrated that good results on a hydrological model could be achieved with a particle filter with about 200 members. However, this is substantially more computationally expensive than an EnKF, which typically requires about 20 members to overcome sampling error problems for LSMs (Maggioni et al., 2012; Carrera et al., 2015; Fairbairn et al., 2015). Moreover, particle filters are much less effective when there are significant model and forcing errors because the non-Gaussian pdf they generate is no longer accurate.

Finally, in order to be consistent with Draper et al. (2011) and to demonstrate known deficiencies in the radiative forcing, we used the original version of SIM in our study. The original version of SIM has recently been upgraded to incorporate a direct bias-correction of the underestimated radiative forcing, the multi-layer ISBA-DIF land surface model and the introduction of a sub-grid scale hydrogeological model specifically for mountainous regions. The bias-correction of the radiative forcing is not homogeneous as in our experiments, but varies depending on the altitude and the cloud cover. A comparison of the original and new versions of SIM is expected to be published shortly (Patrick Le Moigne, personal communication). Furthermore, in our experiments we did not perform the DA for the regions in the SIM domain outside of France (shown in Fig. 2). Instead these regions used the model drainage and runoff. This would not have influenced the WG1 and LAI scores over France because SURFEX does not model horizontal exchanges. However, the MODCOU river discharge in the Rhone basin in southeast France is partly influenced by mountain rivers in Switzerland (Habets et al., 2008). Given that the modelled discharge in this



region is generally unreliable because of the numerous dams, we would not expect the assimilation of data over Switzerland to substantially change the results in this study. In future applications we intend to use the new version of SIM with an extension of LDAS to the full SIM domain.

5 Conclusions

5 This article has examined the impact of assimilating SSM and LAI observations with an SEKF on the SIM hydrological model. To our knowledge, this is the first article to perform an integrated validation of LAI assimilation using a hydrological model. Previous work has demonstrated that the SAFRAN atmospheric forcing underestimates short-wave and long-wave radiation by approximately 5% averaged over France. We found in this study that the ISBA-A-gs model significantly underestimates the LAI for grasslands in winter compared with the observations. These issues result in an underestimation (overestimation) of
10 evapotranspiration (drainage and runoff). The excess water flowing into the rivers and aquifers contributes to an overestimation of the SIM river discharge.

We tried to overcome these problems with four different experiments: (i) a correction of the grassland minimum value from $0.3\text{m}^2/\text{m}^2$ to $1.2\text{m}^2/\text{m}^2$ over France, (ii) a homogeneous bias-correction of the direct radiative forcing (+5%) over France, (iii) the assimilation of LAI observations and (iv) the assimilation of SSM and LAI observations. The DA for (iii) and (iv) was
15 performed with the SEKF, which uses finite differences in the Jacobian calculations in order to extract information from the observations to the prognostic variables (LAI and WG2). The assimilation of SSM observations in experiment (iv) would not be expected to significantly reduce the errors caused by the systematic model and forcing deficiencies because the observations are scaled such that the mean and standard deviation match the model climatology. Nevertheless, it is designed to correct short term errors in SSM and should therefore influence SIM.

20 Experiment (i) improved the SIM Nash scores by 12% because increasing the LAI minimum results in greater evapotranspiration in winter/spring, which subsequently reduces the drainage and runoff fluxes. Furthermore, experiment (ii) enhanced the Nash scores by 20% because increasing the radiative forcing significantly increases evapotranspiration during much of the year, which also reduces the drainage and runoff fluxes. Despite considerably reducing the LAI phase errors, experiment (iii) had a relatively small impact on the discharge Nash efficiency of SIM, improving the efficiency by just 2%. This can be
25 explained by the SEKF LAI Jacobian, which spreads information from the LAI observations to the LAI prognostic variable. In accordance with Rüdiger et al. (2010), the LAI Jacobian values vary seasonally and are generally small in winter and spring. The LAI minimum is significantly underestimated in winter, but the small Jacobians dampen the analysis increment during this period and therefore prevent any significant correction. These Jacobians are physically reasonable because the vegetation is dormant in winter. The main problem is the underlying assumption made by the SEKF that the model is perfect.

30 Experiment (iv) resulted in spurious increases in drainage and runoff, which degraded the SIM discharge Nash efficiency by about 35%. In accordance with Draper et al. (2011), this problem can be traced back to the SEKF Jacobian linking WG1 with WG2. This Jacobian value is negatively correlated with WG1 itself. This results in large analysis increments when rainfall is detected in the surface soil moisture observations but is missed by the model, and small increments when rainfall is detected



by the model but is missed by the soil moisture observations. This imbalance leads to a build up of water in the WG2 analysis that is then lost through drainage and runoff, inducing a positive bias in the SIM discharge. The main problem is that the SEKF cannot account for model and precipitation errors. This motivates the development of an ensemble Kalman filter (EnKF) because it can stochastically capture these errors in the ensemble spread. An EnKF with this capability is currently being
5 developed at Météo-France. It should also be possible to improve the coupling between the surface and root-zone model layers with a new multi-layer diffusion model and the multi-energy balance version.

Finally, the results highlight the important role that vegetation plays on the hydrological cycle. The correction of the LAI minimum in this study was based on a rather arbitrary homogeneous value of $1.2\text{m}^2/\text{m}^2$. Work is already underway to provide a more realistic and spatially variable LAI minimum for grasslands based on observations.

10 *Author contributions.* TEXT

Acknowledgements. This work is a contribution to the IMAGINES (grant agreement 311766) project, co-funded by the European Commission within the Copernicus initiative in FP7. The work was also funded by the EUMETSAT H-SAF service. Discussions with Patrick Le Moigne were useful for understanding the SIM hydrological model. Useful feedback was also obtained through discussions with DA scientists at the Met Office.



References

- Albergel, C., Calvet, J.-C., Mahfouf, J.-F., Rüdiger, C., Barbu, A., Lafont, S., Roujean, J.-L., Walker, J., Crapeau, M., and Wigneron, J.-P.: Monitoring of water and carbon fluxes using a land data assimilation system: a case study for southwestern France, *Hydrol. Earth Syst. Sci.*, 14, 1109–1124, doi:10.5194/hess-14-1109-2010, 2010a.
- 5 Albergel, C., Calvet, J.-C., de Rosnay, P., Balsamo, G., Wagner, W., Hasenauer, S., Naeimi, V., Martin, E., Bazile, E., Bouysse, F., and Mahfouf, J.-F.: Cross-evaluation of modelled and remotely sensed surface soil moisture with in situ data in southwestern France, *Hydrol. Earth Syst. Sci.*, 14, 2177–2191, doi:10.5194/hess-14-2177-2010, 2010b.
- Barbu, A., Calvet, J., Mahfouf, J., Albergel, C., and Lafont, S.: Assimilation of Soil Wetness Index and Leaf Area Index into the ISBA-A-gs land surface model: grassland case study, *Biogeosciences*, 8, 1971–1986, doi:10.1002/qj.339, 2011.
- 10 Barbu, A., Calvet, J., Mahfouf, J., and Lafont, S.: Integrating ASCAT surface soil moisture and GEOV1 leaf area index into the SURFEX modelling platform: a land data assimilation application over France, *Hydrol. Earth Syst. Sci.*, 18, 173–192, doi:10.5194/hess-18-173-2014, 2014.
- Baret, F., Weiss, M., Lacaze, R., Camacho, F., Makhmared, H., Pacholczyk, P., and Smetse, B.: GEOV1: LAI and FAPAR essential climate variables and FCOVER global time series capitalizing over existing products. Part I: Principles of development and production, *Remote Sens. Environ.*, 137, 299–309, 2013.
- 15 Bartalis, Z., Wagner, W., Naeimi, V., Hasenauer, S., Scipal, K., Bonekamp, H., Figa, J., and Anderson, C.: Initial soil moisture retrievals from the METOP-A Advanced Scatterometer (ASCAT), *Geophys. Res. Lett.*, 34, 10.1029/2007GL031088, 2007.
- Boone, A., Calvet, J.-C., and Noilhan, J.: Inclusion of a Third Soil Layer in a Land Surface Scheme Using the Force–Restore Method, *J. Appl. Meteor.*, 38, 1611–1630, 1999.
- 20 Brut, A., Rüdiger, C., Lafont, S., Roujean, J.-L., Calvet, J.-C., Jarlan, L., Gibelin, A.-L., Albergel, C., Moigne, P. L., Soussana, J.-F., Klumpp, K., Guyon, D., Wigneron, J.-P., and Ceschia, E.: Modelling LAI at a regional scale with ISBA-A-gs: comparison with satellite-derived LAI over southwestern France, *Biogeosciences*, 6, 1389–1404, 2009.
- Calvet, J.-C. and Noilhan, J.: From Near-Surface to Root-Zone Soil Moisture Using Year-Round Data, *J. Hydrometeorol.*, 1, 393–411, 2000.
- Calvet, J.-C., Noilhan, J., Roujean, J.-L., Bessemoulin, P., Cabelguenne, M., Olioso, A., and Wigneron, J.-P.: An interactive vegetation SVAT model tested against data from six contrasting sites, *Agric. For. Meteorol.*, 126, 73–95, 1998.
- 25 Carrera, M., Bélair, S., and Bilodeau, B.: The Canadian Land Data Assimilation System (CaLDAS): Description and Synthetic Evaluation Study, *J. Hydrometeorol.*, 16, 1293–1294, doi:http://dx.doi.org/10.1175/JHM-D-14-0089.1, 2015.
- Crow, W. and Wood, E.: The assimilation of remotely sensed soil brightness temperature imagery into a land surface model using Ensemble Kalman filtering., *Adv. Water Resour.*, 26, 137–149, 2003.
- 30 de Rosnay, P., Drusch, M., Vasiljevic, D., Balsamo, G., Albergel, C., and Isaksen, L.: A simplified Extended Kalman Filter for the global operational soil moisture analysis at ECMWF, *Q. J. R. Meteorol. Soc.*, 139, 1199–1213, doi:10.1002/qj.2023, 2013.
- Deardorff, J.: A parameterization of ground surface moisture for use in atmospheric prediction models, *J. Appl. Meteorol.*, 16, 1182–1185, 1977.
- Decharme, B., Boone, A., Delire, C., and Noilhan, J.: Local evaluation of the Interaction between Soil Biosphere Atmosphere soil multilayer diffusion scheme using four pedotransfer functions, *J. Geophys. Res.*, 116, D20 126, doi:10.1029/2011JD016002, 2011.
- 35 Draper, C., Mahfouf, J.-F., and Walker, J.: An EKF assimilation of AMSR-E soil moisture into the ISBA surface scheme, *Journal of Geophysical Research*, 114, D20 104, doi:10.1029/2008JD011650, 2009.



- Draper, C., Mahfouf, J.-F., Calvet, J.-C., Martin, E., and Wagner, W.: Assimilation of ASCAT near-surface soil moisture into the SIM hydrological model over France, *Hydrol. Earth Syst. Sci.*, 15, 3829–3841, doi:10.5194/hess-15-3829-2011, 2011.
- Draper, C., Reichle, R., Lannoy, G. D., and Liu, Q.: Assimilation of passive and active microwave soil moisture retrievals, *Geophys. Res. Lett.*, 39, L04 401, doi:10.1029/2011GL050655, 2012.
- 5 Drusch, M. and Viterbo, P.: Assimilation of screen level variables in ECMWF's Integrated Forecast system: A study on the Impact on the Forecast Quality and Analyzed Soil Moisture., *Mon. Wea. Rev.*, 135 (2), 300–314, doi:10.1175/MWR3309.1, 2007.
- Drusch, M., Wood, M., and Gao, H.: Observation operators for the direct assimilation of TRMM Microwave Imager retrieved soil moisture., *Geophys. Res. Lett.*, 32, L15 403, doi:10.1029/2005GL0236, 2005.
- Duerinckx, A., Hamdi, R., Mahfouf, J.-F., and Termonia, P.: Study of the Jacobian of an extended Kalman filter for soil analysis in SUR-
10 FEXv5, *Geosci. Model Dev.*, 8, 845–863, doi:10.5194/gmd-8-845-2015, 2015.
- Durand, Y., Brun, E., Mérindol, L., Gilbert, G., Bernard, L., and Martin, E.: A meteorological estimation of relevant parameters for snow models, *Ann. of Glaciol.*, 18, 65–71, 1993.
- Entekhabi, D. et al.: The Soil Moisture Active Passive (SMAP) Mission, *Proceedings of the IEEE* 98.5 (2010): 704-716. © Copyright 2010 IEEE, 2010.
- 15 Evensen, G.: Sequential data assimilation with a nonlinear quasi-geostrophic model using Monte Carlo methods to forecast error statistics, *J. Geophys. Res.*, 99, 10 143–10 162, 1994.
- Fairbairn, D., Barbu, A., J.-F. Mahfouf, J.-C. C., and Gelati, E.: Comparing the ensemble and extended Kalman filters for in situ soil moisture assimilation with contrasting conditions, *Hydrol. Earth. Syst. Sci.*, 19, 4811–4830, doi:10.5194/hess-19-4811-2015, 2015, 2015.
- Faroux, S., Tchuente, A. K., Roujean, J.-L., Masson, V., Martin, E., and Moigne, P. L.: ECOCLIMAP-II/Europe: a twofold database of
20 ecosystems and surface parameters at 1 km resolution based on satellite information for use in land surface, meteorological and climate models, *Geosci. Model Dev.*, 6, 563–582, doi:10.5194/gmd-6-563-2013, 2013.
- Gibelin, A.-L., Calvet, J.-C., Roujean, J.-L., Jarlan, L., and Los, S.: Ability of the land surface model ISBA-A-gs to simulate leaf area index at the global scale: Comparison with satellites products, *J. Geophys. Res.*, 111, D18 102, doi:10.1029/2005JD006691, 2006.
- Habets, F., Boone, A., Champeaux, J. L., Etchevers, P., Franchistéguy, L., Leblois, E., Ledoux, E., Moigne, P. L., Martin, E., Morel, S.,
25 Noilhan, J., Segui, P. Q., Rousset-Regimbeau, F., and Viennot, P.: The SAFRAN-ISBA-MODCOU hydrometeorological model applied over France, *J. Geophys. Res.*, 113, D06 113, 2008.
- Houser, P., Shuttleworth, W., Famiglietti, J., Gupta, H., Syed, K., and Goodrich, D.: Assessment of a multi-dimensional satellite rainfall error model for ensemble generation of satellite rainfall data, *Water Resour. Res.*, 34, 3405–3420, 1998.
- Jarlan, L., Balsamo, G., Lafont, S., Beljaars, A., and Calvet, J.-C.: Analysis of leaf area index in the ECMWF land surface model and impact
30 of latent heat on carbon fluxes: application to West Africa, *J. Geophys. Res.*, 113, D24 117, 2008.
- Jazwinski, A. H.: *Stochastic Processes and Filtering Theory*, pp. 150–158, Academic press, 1970.
- Kerr, Y. H., Waldteufel, P., Wigneron, J.-P., Martinuzzi, J.-M., Font, J., and Berger, M.: Soil moisture retrieval from space: the Soil Moisture and Ocean Salinity (SMOS) mission, *Transactions on Geoscience and Remote Sensing*, 39, 1729–1735, 2001.
- Koster, R. and Suarez, M.: Modeling the land surface boundary in climate modls as a composite of independent vegetationstands, *J. Geophys. Res.*, 97, 2697–2715, 1992.
- 35 Ledoux, E., Girard, G., Marsily, G. D., and Deschenes, J.: Spatially distributed modeling: Conceptual approach, coupling surface water and ground water, in: *Unsaturated Flow Hydrologic Modeling: Theory and Practice*, NATO, ASI Series C, edited by Morel-Seytoux, H., vol. 275, pp. 435–454, 1989.



- Maggioni, V., Anagnostou, E., and Reichle, R.: The impact of model and rainfall forcing errors on characterizing soil moisture uncertainty in land surface modeling, *Hydrol. Earth. Syst. Sci.*, 16, 3499–3515, doi:10.5194/hess-16-3499-2012, 2012.
- Mahfouf, J.: Advances in model physics and their relevance to satellite data assimilation, Proceedings of the ECMWF seminar on the use of satellite observations in NWP, http://www.ecmwf.int/sites/default/files/MAHFOUF_ECMWF2014_web.pdf, last accessed September 5 2014, 2014.
- Mahfouf, J.-F. and Noilhan, J.: Inclusion of gravitational drainage in a land surface scheme based on the force-restore method, *J. Appl. Meteorol.*, 35, 987–992, 1996.
- Mahfouf, J.-F., Bergaoui, K., Draper, C., Bouyssel, C., Taillefer, F., and Taseva, L.: A comparison of two off-line soil analysis schemes for assimilation of screen-level observations, *J. Geophys. Res.*, 114, D08 105, doi:10.1029/2008JD011077, 2009.
- 10 Masson, V. et al.: The SURFEXv7.2 land and ocean surface platform for coupled or offline simulation of earth surface variables and fluxes, *Geosci. Model Dev.*, 6, 929–960, doi:10.5194/gmd-6-929-2013, 2013.
- Moradkhani, H., DeChant, C. M., and Sorooshian, S.: Evolution of ensemble data assimilation for uncertainty quantification using the Particle Filter-Markov Chain Monte Carlo method, *Water Resour. Res.*, 48, W2520, doi:10.1029/2012WR012144, 20, 2012.
- Muñoz Sabater, J., Rüdiger, C., Fritz, N., and Kerr, Y.: Joint assimilation of surface soil moisture and LAI observations into a land surface 15 model, *Agricultural and Forest Meteorology*, 148, 1362–1373, doi:10.1016/j.agrformet.2008.04.003, 2008.
- Nash, J. and Sutcliffe, J.: River flow forecasting through conceptual models, Part I - A discussion of principles, *J. Hydrol.*, 10, 282–290, 1970.
- Noilhan, J. and Mahfouf, J.-F.: The ISBA land surface parameterisation scheme, *Global and Planetary Change*, 13, 145–159, 1996.
- Parrens, M., Mahfouf, J.-F., Barbu, A. L., and Calvet, J.-C.: Assimilation of surface soil moisture into a multilayer soil model: design and 20 evaluation at local scale, *Hydrol. Earth Syst. Sci.*, 18, 673–689, 2014.
- Quitana-Ségui, P., Moigne, P. L., Durand, P., Martin, E., Baillon, F. H. M., Canellas, C., and Franchistéguy, L.: Analysis of near-surface atmospheric variables: Validation of SAFRAN analysis over France, *J. Appl. Meteorol. Climatol.*, 47, 92–107, 2008.
- Reichle, R. and Koster, R.: Global assimilation of satellite surface soil moisture retrievals into the NASA Catchment Land Model, *Geophys. Res. Lett.*, 32, L02 404, doi:10.1029/2004GL021700, 2005.
- 25 Reichle, R., Koster, R., Dong, J., and Berg, A.: Global Soil Moisture from Satellite Observations, Land Surface Models, and Ground Data: Implications for Data Assimilation, *J. Hydrometeorol.*, 5, 430–442, 2004.
- Rüdiger, C., Albergel, C., Mahfouf, J.-F., Calvet, J.-C., and Walker, J.: Evaluation of the observation operator Jacobian for leaf area index data assimilation with an extended Kalman filter, *Journal of Geophysical Research*, 115, D09 111, doi:10.1029/2009JD012912, 2010.
- Scipal, K., Drusch, M., and Wagner, W.: Assimilation of a ERS scatterometer derived soil moisture index in the ECMWF numerical weather 30 prediction system, *Adv. Water. Resour.*, 31, 1101–1112, doi:10.1016/j.advwatres.2008.04.013, 2008.
- Scott, D.: *Multivariate Density Estimation: Theory, Practice, and Visualization*, John Wiley & Sons, New York, Chichester, 1992.
- Szczypta, C., Calvet, J.-C., Albergel, C., Balsamo, G., Bousetta, S., Carrer, D., Lafont, S., and Meurey, C.: Verification of the new ECMWF ERA-Interim reanalysis over France, *Hydrol. Earth Syst. Sci.*, 15, 647–666, doi:10.5194/hess-15-647-2011, 2011.
- Vidal, J.-P., Martin, E., Franchistéguy, L., Baillon, M., and Soubeyroux, J.-M.: A 50-year high-resolution atmospheric analysis over France 35 with the Safran system, *Int. J. Climatol.*, 30, 1627–1644, doi:10.1002/joc.2003, 2010.
- Wagner, W., Lemoine, G., and Rott, H.: A method for estimating soil moisture from ERS scatterometer and soil data, *Remote Sens. Environ.*, 70, 191–207, 1999.

Hydrol. Earth Syst. Sci. Discuss., doi:10.5194/hess-2016-195, 2016

Manuscript under review for journal Hydrol. Earth Syst. Sci.

Published: 9 May 2016

© Author(s) 2016. CC-BY 3.0 License.



Wagner, W., Blöschl, G., Pampaloni, P., Calvet, J.-C., Bizzarri, B., Wigneron, J.-P., and Kerr, Y.: Operational Readiness of Microwave Remote Sensing of Soil Moisture for Hydrologic Applications, *Nordic hydrology*, 38, 1–20, doi:10.2166/nh.2007.029, 2007.



Table 1. List of experiments. The bias-correct forcing option implies an increase of the direct short-wave and long-wave radiation by 5%. The SSM outliers removal applies to SSM observations outside the 90% confidence interval of the model.

Experiment	LAI grassland min (m ² /m ²)	Bias-correct forcing	DA	SSM outliers removal
NIT	0.3	No	No	–
NIT _m	1.2	No	No	–
NIT _{bc}	1.2	Yes	No	–
LDAS1	0.3	No	LAI	–
LDAS2	0.3	No	LAI+SSM	No
LDAS1 _{bc}	1.2	Yes	LAI	–
LDAS2 _{bc}	1.2	Yes	LAI+SSM	No
LDAS2 _{QC}	0.3	No	LAI+SSM	Yes



Table 2. Scores for LAI (prognostic variable compared with observations) averaged over 2007-2014. The closest fit to the observations is shown in bold font.

Experiment	RMSD (m ² /m ²)	CC	Bias (m ² /m ²)
NIT	1.18	0.56	0.11
NIT _m	1.14	0.58	0.25
NIT _{bc}	1.02	0.63	0.17
LDAS1	0.69	0.82	-0.08
LDAS2	0.74	0.79	-0.04
LDAS1 _{bc}	0.63	0.84	-0.04
LDAS2 _{bc}	0.69	0.81	-0.02
LDAS2 _{QC}	0.74	0.80	0.01



Table 3. Scores for WG1 (prognostic variable compared with observations) averaged over 2007-2014. The closest fit to the observations are shown in bold font.

Experiment	RMSD (m ³ /m ³)	CC	Bias (m ³ /m ³)
NIT	0.051	0.77	0.00
NIT _m	0.049	0.77	0.00
NIT _{bc}	0.051	0.77	0.00
LDAS1	0.049	0.77	0.00
LDAS2	0.047	0.79	0.00
LDAS1 _{bc}	0.049	0.77	0.00
LDAS2 _{bc}	0.049	0.79	0.00
LDAS2 _{QC}	0.047	0.79	0.00



Table 4. Discharge scores (SIM discharge compared with observations) calculated over 2007-2014. Results only include the stations where at least one of the experiments has a positive Nash efficiency score. The best scores are shown in bold font.

Experiment	Nash efficiency	Discharge ratio (Q_s/Q_o)
NIT	0.41	1.19
NIT _m	0.46	1.15
NIT _{bc}	0.56	1.02
LDAS1	0.42	1.19
LDAS2	0.26	1.28
LDAS1 _{bc}	0.56	1.02
LDAS2 _{bc}	0.44	1.12
LDAS2 _{QC}	0.25	1.29

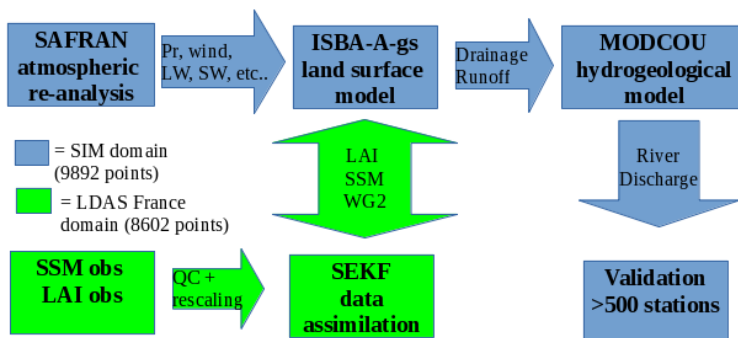


Figure 1. Flowchart of the SIM hydrological model and how LDAS France is connected with SIM.

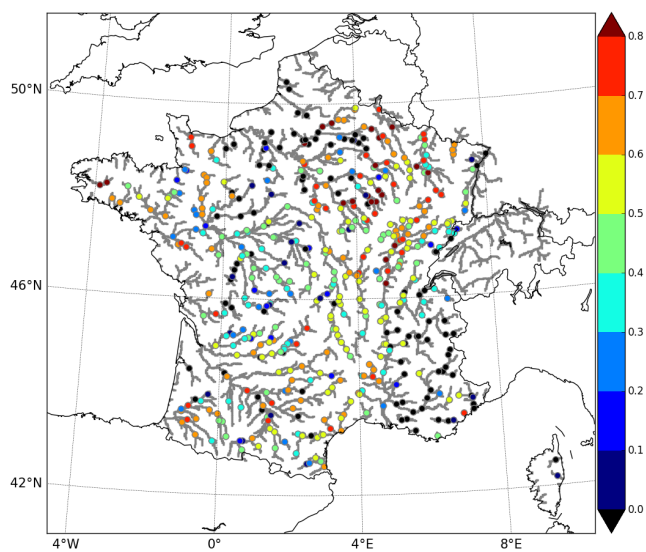


Figure 2. Nash efficiency scores for each station over France for the NIT simulation, calculated over the period 2007-2014. The river network is also shown.

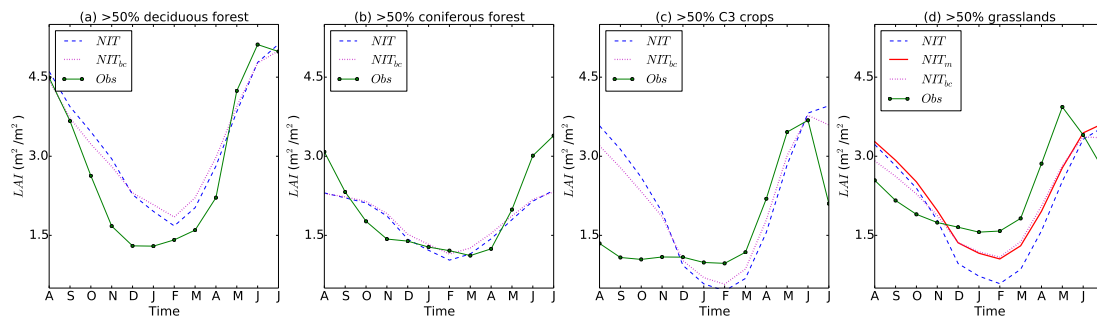


Figure 3. Monthly averaged LAI for the model simulations and for the gridpoints with at least 50% of the four dominant vegetation types, averaged over 2007-2014 and averaged over France.

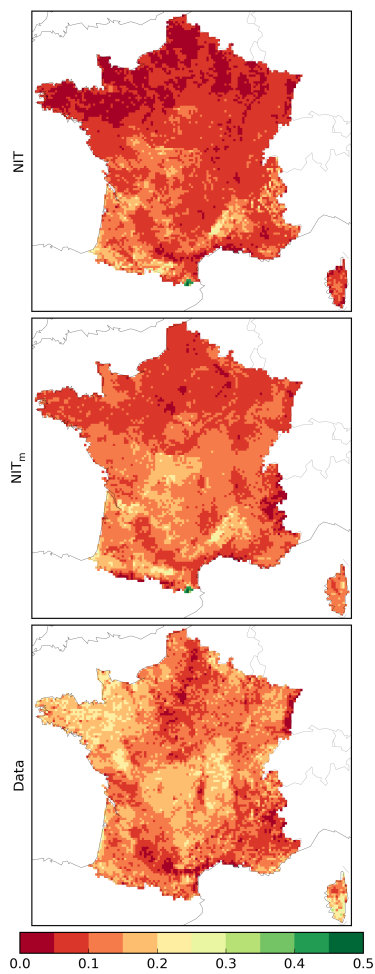


Figure 4. Average annual LAI minimum (2007-2014) for NIT, NIT_m and the observations (m²/m²).

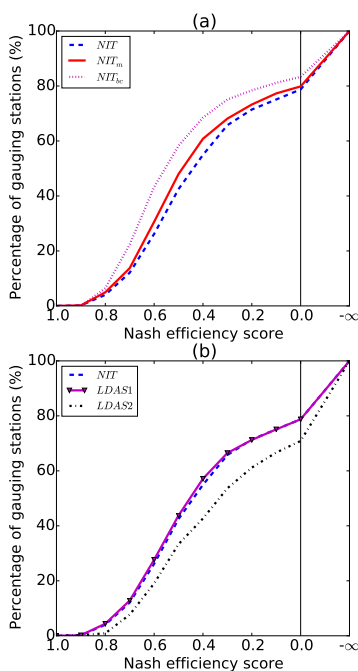


Figure 5. Average Nash efficiency scores over France for (a) the model simulations and (b) the DA methods, calculated over the period 2007-2014. Results only include the stations where at least one of the experiments has a positive Nash efficiency score.

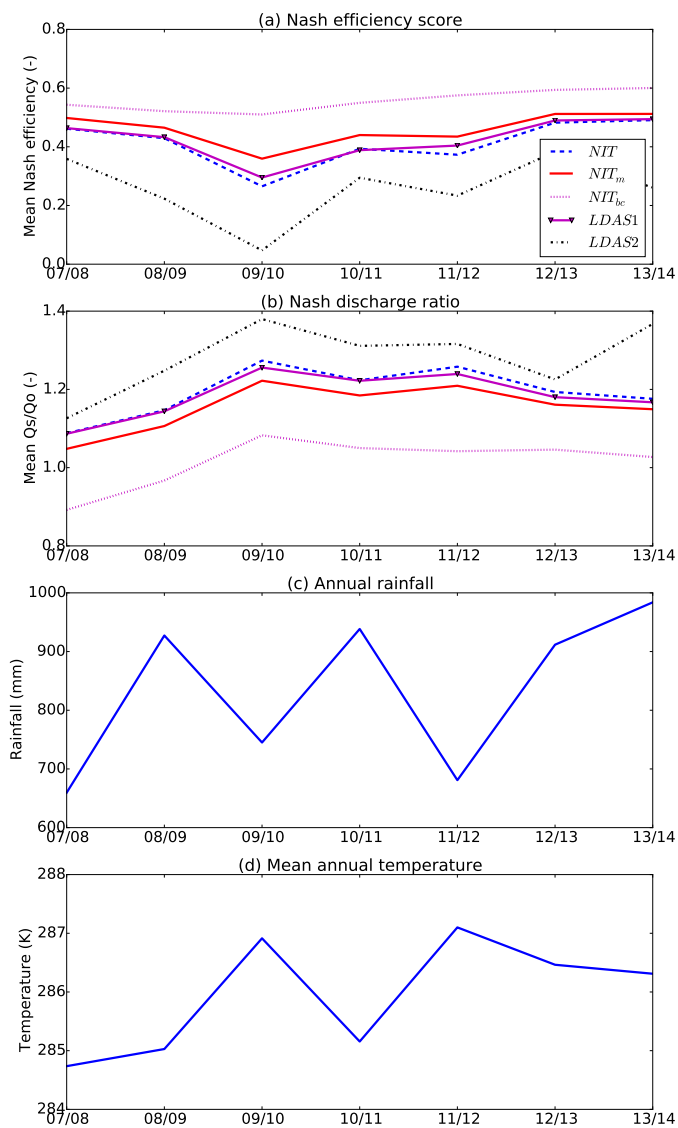


Figure 6. Annual (a) Nash efficiency scores and (b) discharge ratio averaged over France for each experiment. Annual (c) time-averaged temperature and (d) cumulated precipitation averaged over France. Results only include the stations where at least one of the experiments has a positive Nash efficiency score.

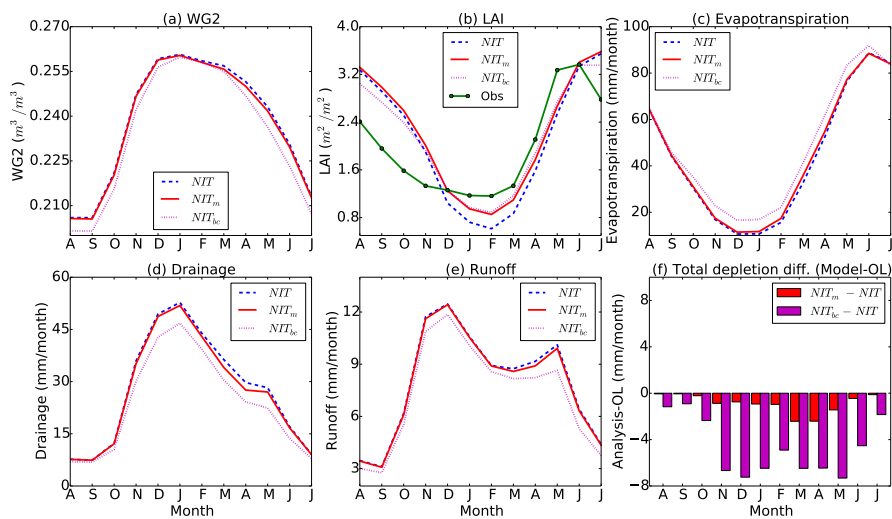


Figure 7. Average monthly (a) WG2 and (b) LAI over France for the model simulations. Monthly cumulative (c) evapotranspiration; (d) drainage and (e) runoff over France for the model simulations. (f) total drainage+runoff differences between NIT and the other model simulations. Results are all averaged over the period 2007-2014.

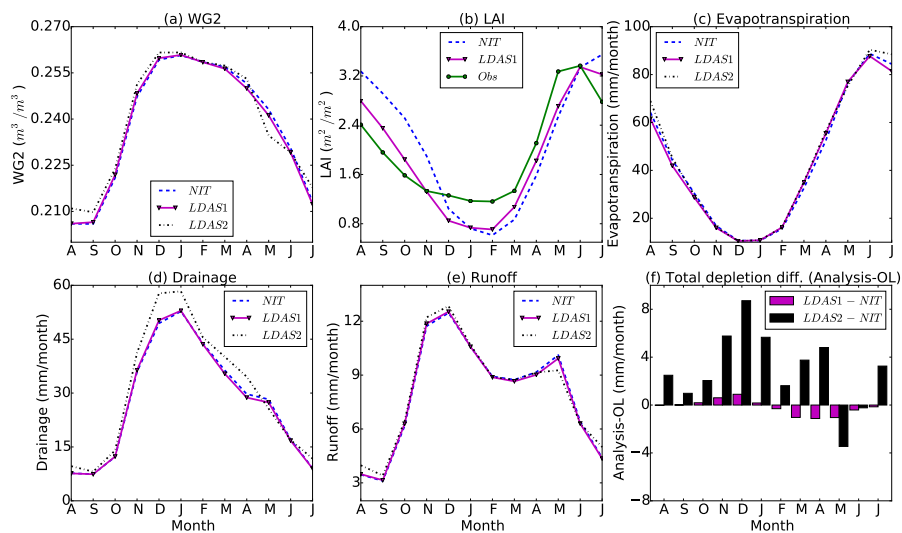


Figure 8. Same as Fig. 7 but LDAS1 and LDAS2 are compared with NIT.

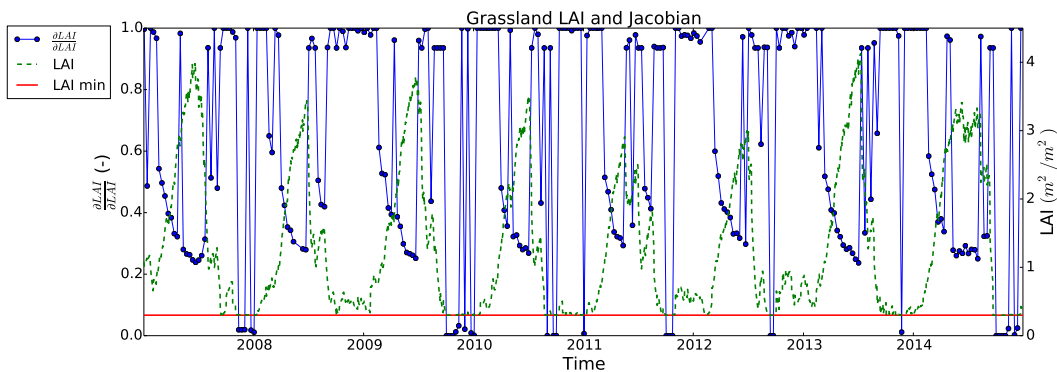


Figure 9. Time evolution of the LDAS1 $\frac{\partial LAI}{\partial LAI}$ Jacobian, together with the LAI analysis and the minimum LAI model parameter for the grassland patch at a point in southwest france (43.35° N, 1.30° E).

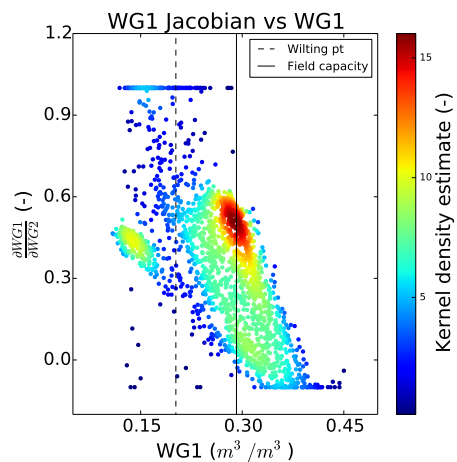


Figure 10. Scatter plot of WG1 against the LDAS2 $\frac{\partial \text{WG1}}{\partial \text{WG2}}$ Jacobian for the grassland patch at the same point as Figure 9.

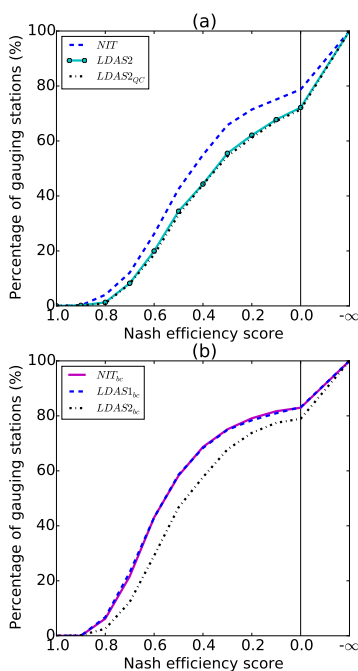


Figure 11. Average Nash efficiency scores over France for (a) the NIT, LDAS2 and LDAS2_{QC} experiments and (b) the NIT_{bc}, LDAS1_{bc} and LDAS2_{bc} experiments.